Applied Surface Science 427 (2018) 687–694

Contents lists available at ScienceDirect

Applied Surface Science

journal homepage: www.elsevier.com/locate/apsusc

Full Length Article

On the nature of citrate-derived surface species on Ag nanoparticles: Insights from X-ray photoelectron spectroscopy

Yuri L. Mikhlin[a,*], Sergey A. Vorobyev[a], Svetlana V. Saikova[b], Elena A. Vishnyakova[a,c], Alexander S. Romanchenko[a], Sergey M. Zharkov[b,d], Yurii V. Larichev[e]

[a] Institute of Chemistry and Chemical Technology of the Siberian Branch of the Russian Academy of Sciences, Akademgorodok 50/24, Krasnoyarsk, 660036, Russia
[b] Siberian Federal University, Svobodny av. 79, Krasnoyarsk, 660041, Russia
[c] Department of Chemistry and The Smalley-Curl Institute, Rice University, 6100 Main Street, Houston, 77005, USA
[d] Kirensky Institute of Physics of the Siberian Branch of the Russian Academy of Sciences, Akademgorodok 50/38, Krasnoyarsk, 660036, Russia
[e] Boreskov Institute of Catalysis of the Siberian Branch of the Russian Academy of Sciences, Lavrent'ev av. 5, Novosibirsk, 630090, Russia

ARTICLE INFO

Article history:
Received 19 June 2017
Received in revised form 30 August 2017
Accepted 5 September 2017
Available online 7 September 2017

Keywords:
Silver nanoparticles
Adsorption
Citrate capping
X-ray photoelectron spectroscopy

ABSTRACT

Citrate is an important stabilizing, reducing, and complexing reagent in the wet chemical synthesis of nanoparticles of silver and other metals, however, the exact nature of adsorbates, and its mechanism of action are still uncertain. Here, we applied X-ray photoelectron spectroscopy, soft X-ray absorption near-edge spectroscopy, and other techniques in order to determine the surface composition and to specify the citrate-related species at Ag nanoparticles immobilized from the dense hydrosol prepared using room-temperature reduction of aqueous Ag^+ ions with ferrous ions and citrate as stabilizer (Carey Lea method). It was found that, contrary to the common view, the species adsorbed on the Ag nanoparticles are, in large part, products of citrate decomposition comprising an alcohol group and one or two carboxylate bound to the surface Ag, and minor unbound carboxylate group; these may also be mixtures of citrate with lower molecular weight anions. No ketone groups were specified, and very minor surface Ag(I) and Fe (mainly, ferric oxyhydroxides) species were detected. Moreover, the adsorbates were different at AgNPs having various size and shape. The relation between the capping and the particle growth, colloidal stability of the high-concentration sol and properties of AgNPs is briefly considered.

1. Introduction

The optical, chemical, bioactive, and other unique properties of Ag nanoparticles (AgNPs) and other nanomaterials can be tuned by varying the size, shape, and surface composition, particularly capping ligands [1,2]. Citrate ions are widely utilized in the wet chemical synthesis of silver [3–14], gold [15–21], platinum [22], and other nanoparticles, acting as reducing (direct reduction of aqueous Ag^+ ions by citrate occurs under boiling or hydrothermal conditions [9–13]), complexing, and stabilizing agent, although the precise mechanisms are far from being fully understood. Citrate is a key reagent for the preparation of silver nanoplates, cubes, disks, etc., as the selective adsorption of citrate on Ag (111) facets impedes their growth and promotes the yield of anisotropic particles [12,23–25]. Transformation of rounded AgNPs to anisotropic ones under illumination [26–28] is believed to be due to decomposition of the citrate capping. Under the synthetic conditions, and also upon the biochemical oxidation of citric acid that is vital for aerobic organisms (the Krebs cycle) [29], citrate is known to oxidize to acetonedicarboxylic and acetoacetic acids, other intermediates, and CO_2 as the final product.

The solution-based synthesis and modification of AgNPs typically involve diluted sols (at most 10 mM) due to the restricted colloidal stability. High-concentration fluid dispersions such as inkjet inks can be obtained using large amounts of surfactants or/and polymer stabilizers [30], which generally should be removed to attain required characteristics of materials. The method of reduction of aqueous Ag^+ with ferrous ions in the presence of sodium citrate proposed by Carey Lea [3] as long ago as 1889 is still a rare example of metal colloids stable up to 1 M concentration without high-molecular-weight reagents [4–10]. It has been reported [5–7] that the AgNPs are negatively charged due to adsorption of citrate anions, and their behavior obeys the Derjaguin-Landau-Verwey-Overbeek (DLVO) model, but the studies have been performed for

* Corresponding author.
E-mail address: yumikh@icct.ru (Y.L. Mikhlin).

http://dx.doi.org/10.1016/j.apsusc.2017.09.026
0169-4332/

diluted solutions, and the reasons behind stability of the dense sols remain elusive. Several forms of citrate bonded to the Ag surface through carboxylate groups have been proposed mainly on the base of surface-enhanced Raman scattering (SERS) [8–12,23], and DFT simulation [24,25]. A hydrogen bond involving an alcohol hydroxyl group has been suggested too, while oxidized derivatives of citrate have been observed on the AgNPs only after heating in air [9,10]. In general, however, the results on the surface composition of nanosilver are still scarce and inconclusive, in particular as SERS is not appropriate for quantitative surface analysis.

In this research we attempted to clarify the nature of citrate-related adsorbates at various fractions of AgNPs manufactured using the Carey Lea method, i.e. avoiding direct oxidation of citrate, applying X-ray photoelectron spectroscopy (XPS) in conjunction with soft X-ray absorption near-edge spectroscopy (XANES), and other techniques, as a prerequisite for understanding the properties and behaviour of AgNPs in the synthesis, dense colloids, the environment and biological systems.

2. Experimental details

2.1. Materials and sample preparation

Silver nitrate ($AgNO_3$), iron sulfate ($FeSO_4{\cdot}7H_2O$), trisodium citrate ($Na_3cit{\cdot}2H_2O$), sodium nitrate ($NaNO_3$), and potassium nitrate (KNO_3) were analytical grade and used as received. Deionized water (Millipore Milli-Q grade) was utilized to prepare all the solutions, to redisperse AgNPs and to rinse the samples deposited onto substrates. Silver nanoparticles were synthesized using the Carey Lea method [3,4], slightly modified here. In a typical procedure, 7 mL of $Na_3cit{\cdot}2H_2O$ solution (400 g/L) and 5 mL of freshly prepared $FeSO_4{\cdot}7H_2O$ solution (300 g/L) were mixed, and then 5 mL of $AgNO_3$ solution (100 g/L) was added under agitation at room temperature. The black residue that formed in about 1 h was separated from the supernatant by centrifugation (3000 rpm for 5 min) and redispersed in a portion of fresh water (10 mL). This hydrosol purified from the excessive reagents and soluble products of the reaction was referred in this research as an "initial" sample; the discarded supernatant contained sodium and iron cations, citrate, sulfate and nitrate anions together with minor AgNPs was analyzed as a reference.

The AgNP sol was then fractioned in several ways via coagulation of nanosilver by adding electrolyte solutions ($NaNO_3$ or KNO_3) of various concentrations, centrifugation, and following redispersion of the precipitated gel in water. The samples of two AgNP fractions, which spectra are presented below, were prepared as follows. 5 mL of the initial Carey Lea sol was mixed with 5 mL of 0.5 M KNO_3 solution, resulting in coagulation of less stable colloids, which were centrifuged (3000 rpm, 5 min) and then redispersed in water (5 mL). This sol contained larger particles was referred as sample (i). The supernatant produced by the centrifugation was mixed with 1 M KNO_3 solution (5 mL) to coagulate the next fraction of Ag NPs, which was separated by centrifugation and then redispersed in water (sample ii).

Specimens for XPS, XANES, and scanning electron microscopy were prepared by placing a droplet (10 μL) of the AgNP sols on freshly renewed surface of HOPG, copper foil with a native oxide layer, or some other supports, and drying in air at room temperature. These samples were analyzed as-prepared, and also cautiously rinsed with water and re-analyzed after drying.

2.2. X-ray photoelectron spectroscopy

X-ray photoelectron spectra and X-ray excited Ag $M_{4,5}VV$ Auger spectra were taken with a SPECS instrument equipped with a PHOIBOS 150 MCD 9 hemispherical analyzer at electron take-off angle 90° with the pass energy of 10 eV for high-resolution spectra and 20 eV for survey spectra. The spectra presented in this paper were excited by monochromatic Al Kα irradiation (1486.6 eV) of an X-ray tube. The spectra were also acquired using Mg Kα line (1253.6 eV) in order to avoid possible overlapping of O 1s and Auger Na KLL spectra, and to check reproducibility. The pressure in an analytical chamber was in the range of 10^{-9} mBar. The C 1s, O 1s, Ag 3d spectra were fitted with Gaussian-Lorentzian peak profiles after subtraction of a Shirley-type background utilizing CasaXPS software.

2.3. X-ray absorption near-edge structure

The C K-, O K-, Fe $L_{3,2}$-, Cu $L_{3,2}$, and S $L_{3,2}$-edge XANES spectra were recorded in the total electron yield (TEY) mode measuring the drain current through the specimen with a Keathley picoammeter at room temperature at the Russian–German endstation located at the bending magnet beamline D161 (BESSY II synchrotron facility, Helmholtz Zentrum Berlin). The analyzer chamber pressure was about 10^{-10} mBar, the X-ray spot size on the specimen was about 0.2 mm. The estimated monochromator resolution was better than 0.1 eV, the transmission of the monochromator was accounted for by measuring the TEY of clean Au foil, the energy scales were referred to gaseous Ne K-edge absorption.

XPS and XANES measurements with similarly prepared AgNP colloids, including in different spots of the colloid samples dried at various supports, were repeated 4–6 times and 2–3 times, respectively, and the typical well-reproducible spectra are presented in this contribution. The experiments showed that the effects of a support, which could adsorb citrate-related species, interact with the sols, etc., and possible carbonaceous contamination were not important; only the XANES spectra for Cu foil are presented here as an example. On the other hand, the surface composition varies, as illustrated below, with sample preparation, handling (e.g., centrifugation, washing) and AgNP fractionation in a complicated manner that is worthy of further investigation.

2.4. Transmission and scanning electron microscopy

JEM-2100 transmission electron microscope (JEOL) operating at 200 kV was used for TEM characterization of the Carey Lea hydrosol samples, which were prepared by placing a droplet of a diluted colloid on a carbon coated copper grid and allowing the solution to evaporate at room temperature. The particle size distribution was estimated from micrographs for a minimum of 200 particles. Scanning electron micrographs were obtained utilizing a Hitachi S5500 instrument operated at acceleration voltage of 15 kV.

2.5. Small-angle X-ray scattering, dynamic light scattering and zeta potential measurements

SAXS patterns were acquired from the sols loaded in standard X-ray quartz capillaries (1.5 mm) with Kristalloflex-805 (Siemens) instrument applying Cu K irradiation (λ = 0.154 nm). The SAXS patterns were corrected for X-ray absorption, collimation, and background scattering, particle size distribution functions were calculated for spherical nanoparticles using the indirect Fourier transform algorithm implemented in the GNOM program from the ATSAS package [31].

DLS and zeta potential studies were conducted using Zetasizer Nano ZS spectrometer (Malvern Instruments Ltd) at scattering angle 173° in a folded polystyrene cell or polycarbonate cell with Pd electrodes, typically at 25 °C.

3. Results

3.1. TEM, SEM, SAXS characterization

Fig. 1 shows a representative TEM micrograph of AgNPs from the Carey Lea sol diluted to ~1 g/L Ag, and a SEM image of the as-prepared dense sol (about 100 g/L Ag) deposited onto highly oriented pyrolytic graphite (HOPG) and then rinsed with water. Particle size distribution calculated from the SAXS pattern is also presented. The Ag NPs are mainly spheroids of 10–12 nm with a share of ~5 nm in the diameter, and bigger particles, many of which are nanoplates of 20–50 nm in the lateral dimension. The concentrated sol dried on HOPG forms a multilayer film with some pores exposing the substrate.

3.2. XPS characterization

The XPS spectra from the AgNPs were collected before and after washing the dried residue with water (Fig. 2, spectra *b* and *c*, respectively), and were compared with those (*a*) acquired from the supernatant, which remained after the AgNPs were precipitated from the raw reaction mixture, dessicated on the substrate without washing. The composition of the latter is close to trisodium citrate, with small quantities of Fe, sulfate and nitrate ions, and metallic Ag (see also Table S1, Supplementary Material). For the AgNPs samples separated from the solution, the atomic Ag/Na and Ag/Fe ratios equal to ~20 or more, and increase after washing the samples. The Fe 2p spectrum of the supernatant shows the main Fe $2p_{3/2}$ maximum at the binding energy (BE) of ~709 eV attributable to Fe^{2+} ions, and the intensity at higher BEs can be assigned to smaller quantities of Fe^{3+} ions, which may occur as sulfates, citrate complexes [5,32,33], or/and iron oxyhydroxides [34]. For the immobilized AgNPs, the Fe $2p_{3/2}$ band centered at ~711 eV is characteristic of Fe^{3+}-O species [34], and only minor signal from Fe^{2+} is present. The Ag $3d_{5/2}$ peak at 368.3 eV with a narrow full width at half maximum (FWHM) of 0.894 eV, along with the position of Auger Ag M_5VV maximum at the kinetic energy of 357.7 eV, indicate that silver is in elemental form [14,35,36], while contributions of Ag^+ species are negligible.

The C 1s spectrum from the supernatant (Fig. 2, *a*) exhibits three peaks related to aliphatic carbon (~285 eV) including some adventitious carbon, alcohol (286.7 eV), and carboxylate (288.8 eV) [18,36,37], with their intensity ratio close to 3.2:1:3 (Table S1), in agreement with the citrate composition $^{-}$OOC-CH2-C(OH)COO^{-}-CH2-COO^{-}. The C 1s spectra of the AgNPs immobilized after the solution was rejected by centrifugation are notably different. The band of carboxylate can be fitted with the smaller peak at ~289 eV and the larger one at ~288 eV. The BE of the alcohol group line also decreases by about 0.4 eV, and the intensity ratio of aliphatic carbon, alcohol, and both carboxylate signals changed to 2.6:1:2.2. After the sample has been washed with water, the relative intensity of alcohol carbon increases, the component at 289 eV decreases, and the carboxylate-to-alcohol ratio approaches *ca.* 1. Consequently, the line at ~289 eV can be assigned to carboxylate not bound to Ag, and that at ~288 eV is due to carboxylate binding to surface Ag atoms and accepting electron density from the metal. The low-energy shift of the peak of alcohol group suggests the binding of C-O to Ag too. The peak assigned to aliphatic carbon somewhat grows and shifts towards lower BEs, probably, because of exposing graphite support after washing away a part of AgNPs together with remaining electrolyte. Although the fitting of the overlapping peaks at ~285 eV and ~284.5 eV is not unequivocal, it is possible to deduce that the ratio of aliphatic carbon to carboxylate remains close to 1 and certainly less than 2 for this and all other AgNP samples. This means, in particular, that the contribution of contaminations to the spectra was minor.

These conclusions are in principal agreement with the O 1s spectra, which can be fitted with the peak at 531.1 eV attributable to O atoms in COO^{-} groups, including Na and Fe citrates, and, partially, OH chemisorbed on Ag and/or in iron (hydro)oxides, the component at 532.3 eV from an alcohol group in citrate, and the contributions of adsorbed water and possible ketone at BE higher than 533 eV [14,18,35–37]. The ratio of oxygen in COO^{-} group to that of an alcohol group is close to 3 instead of 6 in citrate. A weak maximum observable sometimes at 529.8 eV (such spectra are not presented in Figures) should be assigned to Fe^{3+} oxyhydroxides rather than silver oxide, judging from the spectra of Ag and the relative intensities of the Fe and O lines.

Essentially the same XPS results were acquired for AgNPs deposited onto a copper foil and other supports (not shown in Figures). The findings signify that a considerable part of the species adsorbed on AgNPs contain one alcohol group, and one or two carboxylate rather than three as the citrate. It is important that the contribution of ketone groups at 287–287.5 eV [36,37], which are commonly accepted to emerge due to oxidation of the –COH group [9–13,20,21,26–29], was very minor if any, in agreement with the SERS data [9,10].

3.3. XANES

Carbon and oxygen species often can be easier resolved in their K-edge XANES spectra [38]. Fig. 3 shows synchrotron radiation excited C K-, O K-, and Fe L-edge XANES measured in the total electron yield (TEY) mode from the Carey Lea nanoparticles deposited onto HOPG and Cu foil, and crystalline trisodium citrate as a reference. The C K-edge spectra are dominated by the resonance at 288.4 eV from electron transitions from C 1s to vacant antibonding π^* states in COO^{-} groups [38]; the peak is much higher and narrower, and its energy is somewhat less for trisodium citrate than for AgNPs. A shoulder at ~287.5 eV should be assigned to aliphatic carbon, and broad maxima near 290 eV are attributable to alcohol groups, while signals from ketone groups expected at 286.1–286.5 eV are negligible. The probing depths of TEY XANES are greater than those of XPS, resulting, in particular, in a higher contribution of HOPG and oxidized Cu to the spectra. So, the maxima at ~285 eV and 291.2 eV, which are rather strong for the HOPG-supported sample, are due to the electron transitions to π^* and σ^* states of sp^2-hybridized carbon in HOPG. The strongest feature in O K-edge XANES is the leading maximum from carboxylate at 532.1 eV; its relative intensity decreases, while the one at ~534 eV from alcohol oxygen atoms increases for AgNPs in comparison with sodium citrate. A signal of oxygen in potential ketone groups (531 eV) is almost absent; the contribution observed at 530–531 eV for Cu foil-supported specimen is due to underlying copper (hydro)oxide. In the Fe $L_{3,2}$-edge spectra, the relative intensities of A and B features are characteristic of Fe(III) ions in octahedral coordination with oxygen, alike Fe_2O_3 or FeOOH, although minor quantities of Fe(II) species may occur too [39,40]. In general, the C K- and O K-edge XANES data basically corroborate the XPS results.

3.4. Surface analysis of different AgNP fractions

One can suggest that some sorts of AgNPs (see the TEM and SEM images in Fig. 1) are preferentially removed by water rinsing, and the changes of the XPS spectra after washing (Fig. 2) are related to distinct species adsorbed on different AgNPs. A complete fractionation of the dense sols is challenging because of an effective interaction and association of the colloidal particles. On this reason, the hydrodynamic diameters determined with DLS were larger than the size determined using TEM and SAXS, and dependent on the sol dilution, concentration of electrolyte employed for the frac-

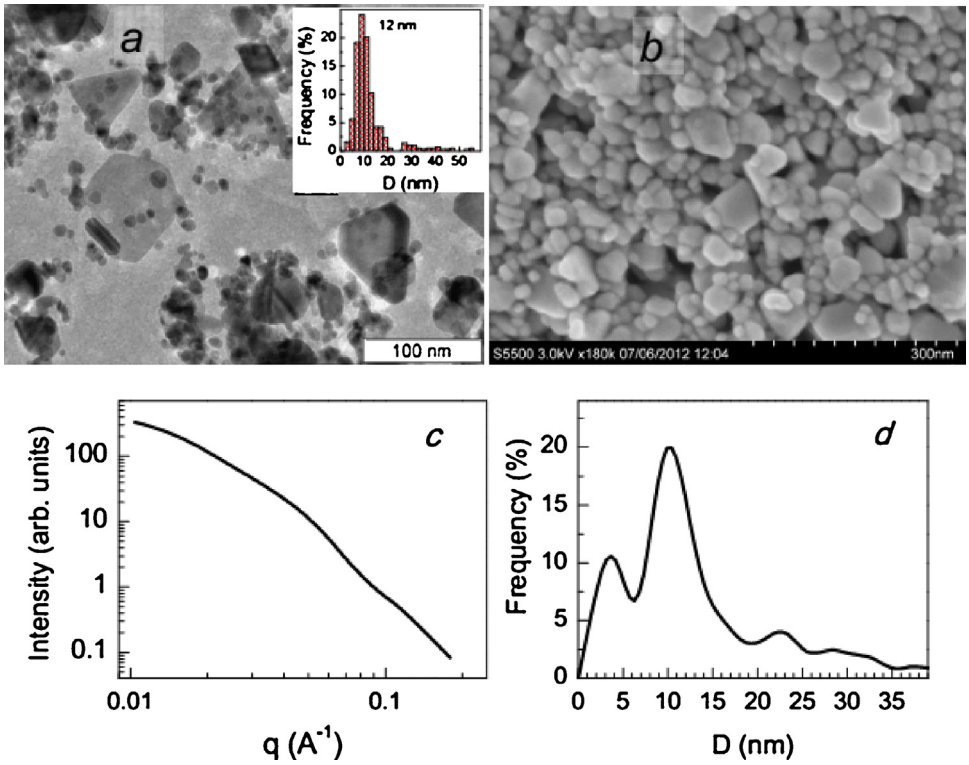

Fig. 1. TEM image (a) of the diluted hydrosol (1 mM Ag), SEM image (b) of the 0.4 M Carey Lea hydrosol dried and then washed on HOPG; (c, d) small-angle X-ray scattering pattern and the relevant particle size distribution, respectively.

tionation, and other factors. For the colloid fractions, which were separated by coagulation of the initial sol adding sodium nitrate (some examples can be seen in Fig. S3, Supplementary Material), the hydrodynamic diameters decrease as more concentrated electrolyte solutions were employed for coagulation. Zeta potentials of AgNPs measured using laser Doppler electrophoresis are negative, and show fairly wide distributions, with the average value ranged from −25 mV to −50 mV for different fractions.

Fig. 4 shows the photoelectron C 1s spectra (more XPS data are given in Supplementary Material) from two fractions of the Carey Lea sol prepared as follows: (i) Ag NPs were separated by electrolytic coagulation with 0.5 M KNO_3 followed by centrifugation, and then redispersion in water; (ii) nanoparticles from the supernatant were coagulated by 1 M KNO_3, centrifuged, and redispersed in fresh water. The C 1s spectrum from the sample (i) dried on HOPG (Fig. 4, *a*) exhibits the carboxylate-to-alcohol ratio of 2.7 that is higher than for the AgNPs before fractioning but is less than for citrate (Fig. 2). The spectrum contains, in addition to the strong signal of Ag-bound carboxylate at 288.2 eV, the component at ~289 eV (30% of total carboxylate), which preserves after washing the sample (spectrum *b*), when the total carboxylate-to-alcohol ratio decreased to 1.7. The intensity of K 2p doublet corresponds to the ratios of total carboxylate and pendant COO^- groups to K^+ of 2.6 and 0.7, respectively (Table S1), and the K signal disappeared after the washing. The amount of Fe was near the detection limit of XPS (carboxylate to Fe ratio greater than ~50).

For the sample (ii) that consists of 5–7 nm particles (TEM image in Fig. 4), the ratio of carboxylate and alcohol groups is ~1, a relative share of the pendant COO^- is small (~10%), and both values insignificantly change after washing (*c* and *d*). The increased quantity of K^+ before the washing operation, which completely removes K and N, is due to potassium nitrate, with the ratio of carboxylate to K^+ being 1.2 after subtraction of the KNO_3 content. The results obtained for the fractions (i) and (ii) suggest that alkali cations are weakly (electrostatically) attached to AgNPs; the cations are probably localized near both unbound COO^- groups and those bound to Ag surface, similar to Na^+ in gold NPs – citrate system [20], albeit some minor citrate salts from the dried solution may still contribute to the spectra.

4. Discussion

4.1. Composition of surface species

The above findings can be explained as follows. Uncompromised citrate anions, which bind to surface Ag atoms via two carboxylate and alcohol oxygen, appear to exist, in a mixture with other adsorbates, on spherical AgNPs of ~10–12 nm (Fig. 5, *a*). The rounded nanoparticles Ag NPs of ~6 nm in diameter are capped with ligands composed of one carboxylate anion and one alcohol group, both bound to the surface Ag atoms, and one or two aliphatic carbon atoms. Fig. 5, *b* exemplifies 3-hydroxybutyrate formed by the removal of two carboxylate groups; the lowest-molecular-weight adsorbates may be hydroxypropionates (see Fig. S4 in Supplementary Material), although this requires C—C bond cleavage. These NPs bear a lower negative charge and tend to association but are more stable towards electrolytic coagulation. The small size of the NPs may be due to dense capping, which impedes attachment of aqueous Ag^+ ions and the crystal growth. Silver nanoplates and rods are preferentially covered with ligands having two carboxylates, either one or two of them bound to Ag atoms together with alcohol oxygen, produced by decarboxylation of citrate (Fig. 5, *c*). Zhang et al. [21] have elucidated that the production of anisotropic Ag particles is promoted, aside from citrate, by reagents containing two carboxylates, which retard the growth of Ag(111) facets, and this seems to be the case for the anisotropic AgNPs in the Carey Lea synthesis. It should be admitted that the exact number of aliphatic carbon atoms (owing to contributions

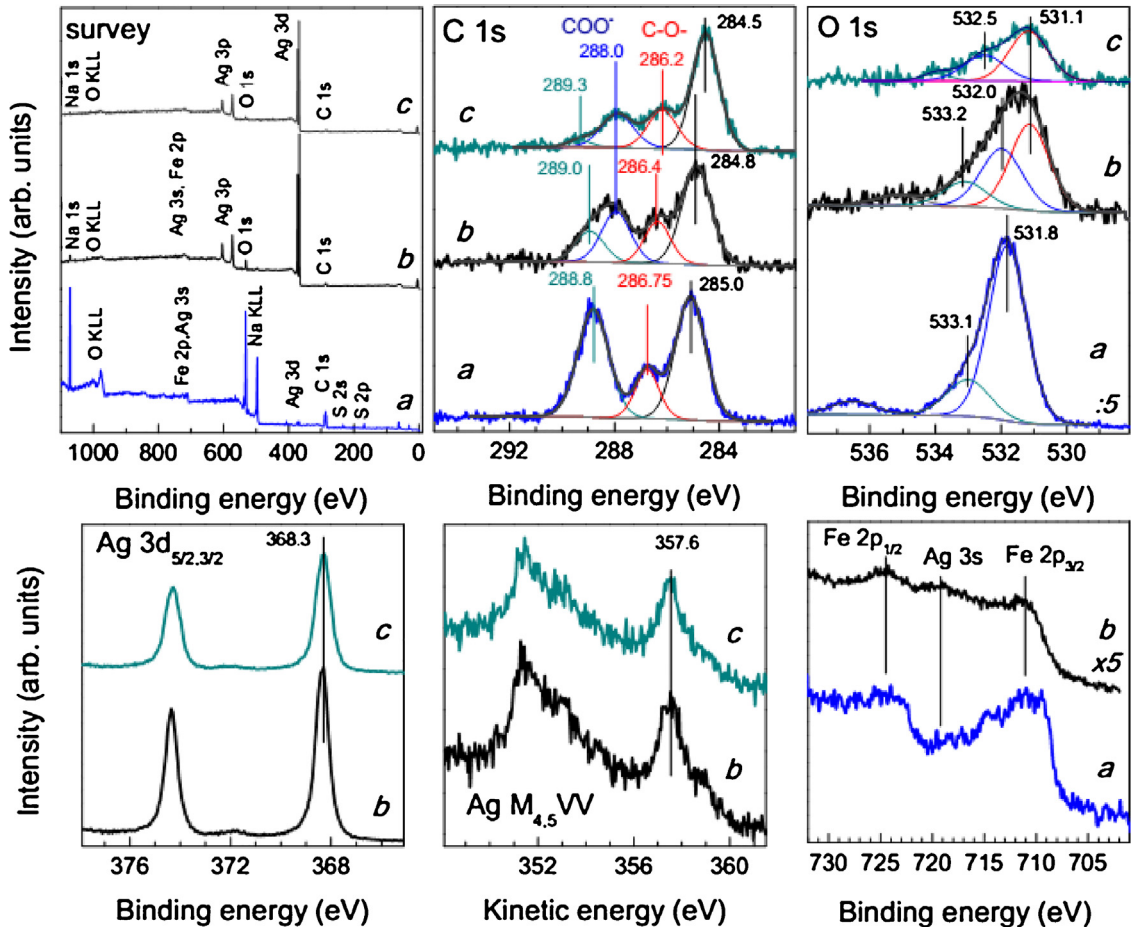

Fig. 2. X-ray photoelectron spectra of dispersion droplets dried on HOPG: (a) supernatant of the reaction mixture, (b) AgNPs separated from the mixture by centrifugation and redispersed in water, and the sample (b) washed with water on HOPG (c).

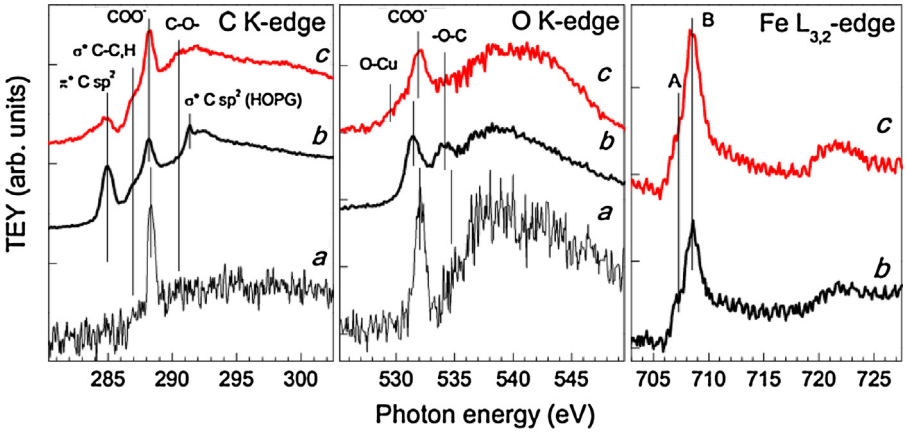

Fig. 3. TEY XANES of (a) trisodium citrate and the Carey Lea sol droplet dried and water washed on (b) HOPG and (c) copper foil.

of adventitious carbon and supports), positions of the functional groups in the adsorbate molecules (taking in mind, in particular, that the formation of isocitrate may precede its oxidation, similar to the biochemical reaction [29]), and details of the binding to Ag cannot be surely specified with XPS, so the structures depicted in Fig. 5 are arbitrary and require further research. Moreover, it is possible that the compositions specified using XPS actually originate from simultaneous presence of two or more molecules; for example, there can be a mixture of citrate and hydroxypropionate instead of the structures shown in Fig. 5, *c*.

4.2. Origin of the citrate-derived ligands

The decomposition of citrate can involve Fe(III) and oxygen as oxidizing agents, and catalytic effect of Ag surface and Fe substances. It is noteworthy that the smaller AgNPs are capped with the lower molecular weight ligands with the carboxylate-to-alcohol ratio of 1, which, therefore, form, possibly via radical reactions [41,42], at early stages of the process, arresting the crystal growth (Fig. 5, *b*). The mechanisms need further study, but, anyway, the reactions are different from those in the solution bulk or living

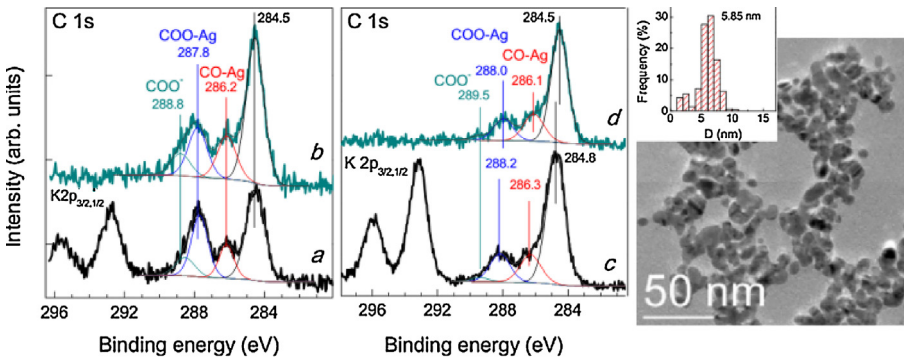

Fig. 4. X-ray photoelectron spectra of sol droplets dried on HOPG (a, b) coagulated with 0.5 M KNO_3, centrifuged and redispersed in water, (c, d) AgNPs coagulated from the supernatant with 1 M KNO_3; (b), (d) samples rinsed with water on HOPG, and TEM image of the sol (c).

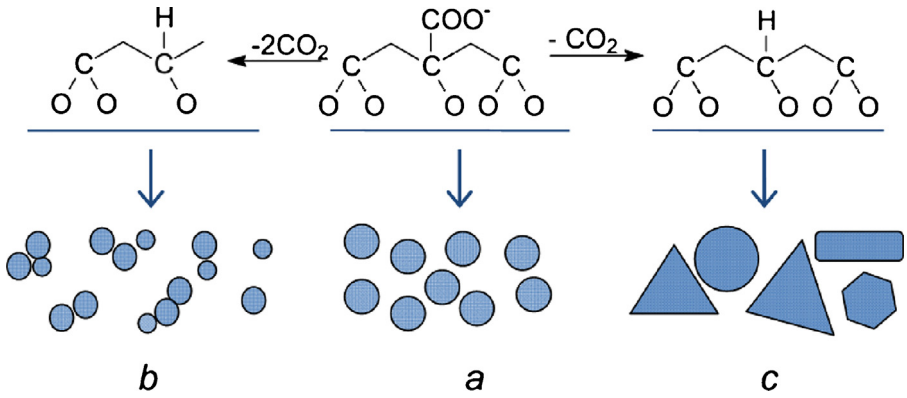

Fig. 5. Scheme illustrating proposed compositions of the citrate-derived surface species on various fractions of AgNPs.

cell mitochondria, which proceed via the stages of oxidation of an alcohol group to ketone as an intermediate, dehydration and decarboxylation [13,26–29]. Conversely, no ketones were found at all the Ag surfaces, and no surface C=O groups have been revealed with *in situ* SERS for the iron-free media too [9,10], probably because of stabilization of alcohol group bound to silver. Li et al. [10], have interpreted the SERS spectra from the bimodal paste composed of ~10 nm and 50 nm AgNPs produced by the Carey Lea and the citrate boiling methods, respectively, in terms of citrate attached to surface Ag atoms via one carboxylate and alcohol hydroxyl; the adsorbed citrate has been suggested to volatilize at 130–180 °C, and ketone groups to form at higher temperatures. Among other things, this confirms that the current XPS findings are not caused by *ex situ* phenomena, and one expects that the surface ligands specified here are similar to those formed in different reactions. It is also interesting that several studies have reported untypical intermediates of the Krebs cycle caused by a silver impact [43,44], implying that AgNPs may disturb the biochemical enzymatic oxidation of citrate by stabilizing the alcohol group as one of the mechanisms of silver toxicity.

4.3. Multimodality and colloidal stability of the Carey Lea hydrosol

The Carey Lea dispersion is comprised of at least three sorts of AgNPs, differing by their size, shape, and surface coating. At the same time, quantities of surface Ag^+, Fe^{2+}/Fe^{3+} citrate complexes and Fe oxyhydroxides are small and unlikely influence the dispersion characteristics, so we hypothesize that the multimodality is the main reason of remarkable colloidal stability of this high-concentration sol. In addition to electrostatic repulsion and van der Waals attraction described by the DLVO theory for uniform particles, more effects take place in multimodal dispersions, including very concentrated ones [45–50]: the repulsion or attraction forces emerge as the space between larger particles depletes with smaller nanoparticles [45,46]; sols can be stabilized by a halo of charged NPs around almost neutral particles [47,49,50]; the structural effects arise from adsorbed NPs confined between the interacting surfaces [48,49]. Up to now, these phenomena have been studied mainly in binary colloidal mixtures of positively charged zirconia NPs and negligibly charged silica spheres and some other suspensions, but metal colloids, to the best of our knowledge, have been never considered in these terms. We may guess that lower surface charge and some hydrophobicity of the AgNPs coated with citrate derivatives, and structuring of AgNPs play a role. Understanding these effects could pave the ways, in particular, for preparation of Ag-based fluid nanodispersions without polymer stabilizers.

5. Conclusions

In summary, the surface analysis based mainly on the photoelectron C 1s spectra revealed that ligands covering the Ag nanoparticles prepared via Fe^{2+}-mediated reduction of Ag^+ are composed of an alcohol group and one or two carboxylate bound to the surface Ag, and minor unbound carboxylate group; alternatively, the adsorbates may represent mixtures of citrate and the products of its decomposition. The surface species differ for various fractions of AgNPs (about 10 nm spheroids, nanoplates, and ~6 nm rounded AgNPs remaining in the supernatant after electrolytic coagulation) probably due to a specific effect of each sort of adsorbates on the crystal growth, rendering the particle size and shape. Ketone groups were absent at for all these nanoparticles because the alcohol was stabilized against oxidation by its binding to Ag. The surface concentrations of iron that occurred as Fe^{3+} oxyhy-

droxides rather than Fe-citrate complexes were minor, particularly after several coagulation-peptization cycles. The fact that the adsorbates are distinct from citrate sheds new light on the behavior of "citrate-stabilized" AgNPs under various conditions, including the formation and colloidal stability of the high-concentration sols.

Acknowledgements

We thank the Russian-German bilateral program "Russian-German laboratory at BESSY II" and the staff of the RGLab and HZB for their kind assistance with XANES experiments.

Appendix A. Supplementary data

Supplementary data associated with this article can be found, in the online version, at http://dx.doi.org/10.1016/j.apsusc.2017.09.026.

References

[1] Yu.A. Krutyakov, A.A. Kudrinskiy, A.Yu. Olenin, G.V. Lisichkin, Synthesis and properties of silver nanoparticles: advances and prospects, Russ. Chem. Rev. 77 (2008) 233–257.
[2] B. Calderón-Jiménez, M.E. Johnson, A.R.M. Bustos, K.E. Murphy, M.R. Winchester, V.R. Baudrit, Silver nanoparticles: technological advances, societal impacts, and metrological challenges, Front. Chem. 5 (2017) 1–26.
[3] M. Carey Lea, Allotropic forms of silver, Am. J. Sci. 37 (1889) 476–491.
[4] G. Frens, J.Th.G. Overbeek, Carey Lea's colloidal silver, Kollod Z. Z. Polym. 233 (1969) 922–929.
[5] J.P. Jolivet, M. Gzara, J. Mazieres, J. Lefebvre, Physicochemical study of aggregation in silver colloids, J. Colloid Interface Sci. 107 (1985) 429–441.
[6] D. Fornasiero, F. Grieser, The kinetics of electrolyte induced aggregation of Carey Lea silver colloids, J. Colloid Interface Sci. 141 (1991) 168–179.
[7] O.V. Dement'eva, A.V. Mal'kovskii, M.A. Filippenko, V.M. Rudoy, Comparative study of the properties of silver hydrosols prepared by citrate and citrate–sulfate procedures, Colloid J. 70 (2008) 561–573.
[8] O. Siiman, L.A. Bumm, R. Callaghan, C.G. Blatchford, M. Kerker, Surface-enhanced Raman scattering by citrate on colloidal silver, J. Phys. Chem. 87 (1983) 1014–1023.
[9] C.H. Munro, W.E. Smith, M. Garner, J. Clarkson, P.C. White, Characterization of the surface of a citrate-reduced colloid optimized for use as a substrate for surface-enhanced resonance raman scattering, Langmuir 11 (1995) 3712–3720.
[10] M. Li, Y. Xiao, Z. Zhang, J. Yu, Bimodal sintered silver nanoparticle paste with ultrahigh thermal conductivity and shear strength for high temperature thermal interface material applications, ACS Appl. Mater. Interfaces 7 (2015) 9157–9168.
[11] A. Henglein, M. Giersig, Formation of colloidal silver nanoparticles: capping action of citrate, J. Phys. Chem. B 103 (1999) 9533–9539.
[12] Z.S. Pillai, P.V. Kamat, What factors control the size and shape of silver nanoparticles in the citrate ion reduction method? J. Phys. Chem. B 108 (2004) 945–951.
[13] S. Patra, A.K. Pandey, D. Sen, S.V. Ramagiri, J.R. Bellare, S. Mazumder, A. Goswami, Redox decomposition of silver citrate complex in nanoscale confinement: an unusual mechanism of formation and growth of silver nanoparticles, Langmuir 30 (2014) 2460–2469.
[14] Y.L. Mikhlin, E.A. Vishnyakova, A.S. Romanchenko, S.V. Saikova, M.N. Likhatski, Y.V. Larichev, F.V. Tuzikov, V.I. Zaikovskii, S.M. Zharkov, Oxidation of Ag nanoparticles in aqueous media: effect of particle size and capping, Appl. Surf. Sci. 297 (2014) 75–83.
[15] J. Turkevich, P.C. Stevenson, J. Hillier, A study of the nucleation and growth processes in the synthesis of colloidal gold, Discuss. Faraday Soc. 11 (1951) 55–75.
[16] Y. Mikhlin, A. Karacharov, M. Likhatski, T. Podlipskaya, Y. Zubavichus, A. Veligzhanin, V. Zaikovski, Submicrometer intermediates in the citrate synthesis of gold nanoparticles: new insights into the nucleation and crystal growth mechanisms, J. Colloid Interface Sci. 362 (2011) 330–336.
[17] M. Doyen, K. Bartik, G. Bruylants, UV-Vis and NMR study of the formation of gold nanoparticles by citrate reduction: observation of gold-citrate aggregates, J. Colloid Interface Sci. 399 (2013) 1–5.
[18] J.-W. Park, J.S. Shumaker-Parry, Structural study of citrate layers on gold nanoparticles: role of intermolecular interactions in stabilizing nanoparticles, J. Am. Chem. Soc. 136 (2014) 1907–1921.
[19] F. Kettemann, A. Birnbaum, S. Witte, M. Wuithschick, N. Pinna, R. Kraehnert, K. Rademann, J. Polte, Missing piece of the mechanism of the Turkevich method: the critical role of citrate protonation, Chem. Mater. 28 (2016) 4072–4081.
[20] H. Al-Johani, E. Abou-Hamad, A. Jedidi, C.M. Widdifield, J. Viger-Gravel, S.S. Sangaru, D. Gajan, D.H. Anjum, S. Ould-Chikh, M. Nejib Hedhili, A. Gurinov, M.J. Kelly, M. El Eter, L. Cavallo, L. Emsley, J.-M. Basset, The structure and binding mode of citrate in the stabilization of gold nanoparticles, Nat. Chem. 9 (2017) 890–895.
[21] D. Grasseschi, R.A. Ando, H.E. Toma, V.M. Zamarion, Unraveling the nature of Turkevich gold nanoparticles: the unexpected role of the dicarboxyketone species, RSC Adv. 5 (2015) 5716–5724.
[22] G.A. Attard, J.-Y. Ye, P. Jenkins, F.J. Vidal-Iglesias, E. Herrero, S.-G. Sun, Citrate adsorption on Pt{h k l} electrodes and its role in the formation of shaped Pt nanoparticles, J. Electroanal. Chem. 688 (2013) 249–256.
[23] Q. Zhang, N. Li, J. Goebl, Z. Lu, Y. Yin, A systematic study of the synthesis of silver nanoplates: is citrate a magic reagent? J. Am. Chem. Soc. 133 (2011) 18931–18939.
[24] D.S. Kilin, O.V. Prezhdo, Y. Xia, Shape-controlled synthesis of silver nanoparticles: ab initio study of preferential surface coordination with citric acid, Chem. Phys. Lett. 458 (2008) 113–116.
[25] G. Mpourmpakis, D.G. Vlachos, Growth mechanisms of metal nanoparticles via first principles, Phys. Rev. Lett. 102 (2009) 155505.
[26] R.C. Jin, Y.C. Cao, E.C. Hao, G.S. Metraux, G.C. Schatz, C.A. Mirkin, Controlling anisotropic nanoparticle growth through plasmon excitation, Nature 425 (2003) 487–490.
[27] G.P. Lee, Y. Shi, E. Lavoie, T. Daeneke, P. Reineck, U.B. Cappel, D.M. Huang, U. Bach, Light-driven transformation processes of anisotropic silver nanoparticles, ACS Nano 7 (2013) 5911–5921.
[28] E.S. Thrall, A.P. Steinberg, X. Wu, L.E. Brus, The role of photon energy and semiconductor substrate in the plasmon-mediated photooxidation of citrate by silver nanoparticles, J. Phys. Chem. C 117 (2013) 26238–26247.
[29] D.L. Nelson, M.M. Cox, Lehninger Principles of Biochemistry, fifth edition, W.H Freeman and company, New York, 2008.
[30] A. Kamyshny, S. Magdassi, Conductive nanomaterials for printed electronics, Small 10 (2014) 3515–3535.
[31] D.I. Svergun, Determination of the regularization parameter in indirect-transform methods using perceptual criteria, J. Appl. Cryst. 25 (1992) 495–503.
[32] I. Gautier-Luneau, C. Merle, D. Phanon, C. Lebrun, F. Biaso, G. Serratrice, J.L. Pierre, New trends in the chemistry of iron (III) citrate complexes: correlations between X-ray structures and solution species probed by electrospray mass spectrometry and kinetics of iron uptake from citrate by iron chelators, Chem. Eur. J. 11 (2005) 2207–2219.
[33] A.M.N. Silva, X. Kong, M.C. Parkin, R. Cammack, R.C. Hider, Iron(III) citrate speciation in aqueous solution, Dalton Trans. 40 (2009) 8616–8625.
[34] M.C. Biesinger, B.P. Payne, A.P. Grosvenor, L.W. Lau, A.R. Gerson, R.S.C. Smart, Resolving surface chemical states in XPS analysis of first row transition metals, oxides and hydroxides: Cr, Mn, Fe, Co and Ni, Appl. Surf. Sci. 257 (2011) 2717–2730.
[35] L.S. Kibis, A.I. Stadnichenko, E.M. Pajetnov, S.V. Koscheev, V.I. Zaykovskii, A.I. Boronin, The investigation of oxidized silver nanoparticles prepared by thermal evaporation and radio-frequency sputtering of metallic silver under oxygen, Appl. Surf. Sci. 257 (2010) 404–413.
[36] I. Mazov, V.L. Kuznetsov, I.A. Simonova, A.I. Stadnichenko, A.V. Ishchenko, A.I. Romanenko, E.N. Tkachev, O.B. Anikeeva, Oxidation behavior of multiwall carbon nanotubes with different diameters and morphology, Appl. Surf. Sci. 258 (2012) 6272–6280.
[37] T.I.T. Okpalugo, P. Papakonstantinou, H. Murphy, J. McLaughlin, N.M.D. Brown, High resolution XPS characterization of chemical functionalised MWCNTs and SWCNTs, Carbon 43 (2005) 153–161.
[38] K. Heymann, J. Lehmann, D. Solomon, M.W.I. Schmidt, T. Regier, C 1 s K-edge near edge X-ray absorption fine structure (NEXAFS) spectroscopy for characterizing functional group chemistry of black carbon, Org. Geochem. 42 (2011) 1055–1064.
[39] P.A. van Aken, B. Liebscher, Quantification of ferrous/ferric ratios in minerals: new evaluation schemes of Fe L_{23} electron energy-loss near-edge spectra, Phys. Chem. Miner. 29 (2002) 188–200.
[40] M. Nagasaka, H. Yuzawa, T. Horigome, A.P. Hitchcock, N. Kosugi, Electrochemical reaction of aqueous iron sulfate solutions studied by Fe L-edge soft X-ray absorption spectroscopy, J. Phys. Chem. C 117 (2013) 16343–16348.
[41] I. Gautier-Luneau, P. Bertet, A. Jeunet, G. Serratrice, J.L. Pierre, Iron-citrate complexes and free radicals generation: is citric acid an innocent additive in foods and drinks, Biometals 20 (2007) 793–796.
[42] X. Ou, X. Quan, S. Chen, F. Zhang, Y. Zhao, Photocatalytic reaction by Fe (III)?citrate complex and its effect on the photodegradation of atrazine in aqueous solution, J. Photochem. Photobiol. A 197 (2008) 382–388.
[43] L. Li, H. Wu, W.J.G.M. Peijnenburg, C.A.M. van Gestel, Both released silver ions and particulate Ag contribute to the toxicity of AgNPs to earthworm *Eisenia Fetida*, Nanotoxicology 9 (2015) 792–801.
[44] J. Carrola, V. Bastos, J.M.P.F. de Oliveira, H. Oliveira, C. Santos, A.M. Gil, I.F. Duarte, Insights into the impact of silver nanoparticles on human keratinocytes metabolism through NMR metabolomics, Arch. Biochem. Biophys. 589 (2016) 53–61.
[45] Y. Mao, M.E. Cates, H.N.W. Lekkerkerker, Depletion force in colloidal systems, Physica A 222 (1995) 10–24.
[46] A. Sharma, J.Y. Walz, Direct measurement of the depletion interaction in a charged colloidal dispersion, J. Chem. Soc. Faraday Trans. 92 (1996) 4997–5004.
[47] F. Zhang, G.G. Long, P.R. Jemian, J. Ilavsky, V.T. Milam, J.A. Lewis, Quantitative measurement of nanoparticle halo formation around colloidal microspheres in binary mixtures, Langmuir 24 (2008) 6504–6508.

[48] C.T. McKee, J.Y. Walz, Interaction forces between colloidal particles in a solution of like-charged, adsorbing nanoparticles, J. Colloid Interface Sci. 365 (2012) 72–80.
[49] J. Lee, S.J. Lee, K.H. Ahn, S.J. Lee, Nanoparticle-induced gelation of bimodal slurries with highly size-asymmetric particles: effect of surface chemistry and concentration, Langmuir 31 (2015) 13639–13646.
[50] F. Zhang, A.J. Allen, L.E. Levine, D.-H. Tsai, J. Ilavsky, Structure and dynamics of bimodal colloidal dispersions in a low-molecular-weight polymer solution, Langmuir 33 (2017) 2817–2828.